

A Theoretical Study on the Factors Influencing Cyanine Photoisomerization: The Case of Thiacyanine in Gas Phase and in Methanol

R. Improta[†] and F. Santoro^{*,‡}

*Istituto di Biostrutture e Biommagini del CNR, via Mezzocannone 6,
I-80134 Napoli, Italy, and Istituto per i Processi Chimico-Fisici del CNR,
Area della Ricerca del CNR di Pisa, via Moruzzi 1, I-56124 Pisa, Italy*

Received November 4, 2004

Abstract: The effects influencing cyanine photoisomerization on the S_1 surface in the condensed phase have been investigated by an integrated quantum mechanical approach, focused mainly on 3,3'-diEt-2,2'-thiacyanine. After excitation, a barrierless motion, involving the torsion coupled to bond skeletal deformation, leads to a slightly nonplanar local C_2 minimum, which we propose to be the fluorescent state. Crossed a barrier of $\approx 120\text{ cm}^{-1}$, a steeper path drives to a more stable C_1 minimum S_1 -Min, corresponding to a pseudoperpendicular twisted intramolecular charge transfer (TICT) state. CAS(6,6) optimization allows for locating the lowest energy S_1/S_0 conical intersection in the isomerization path which is reached from S_1 -Min by an increased asymmetry of the two rings and a marked pyramidalization at one N center. The S_1 surface is rather flat in the Franck–Condon region and suggests that other paths can be competitive with the minimum energy one. The comparison among different cyanines shows how variation of the molecular scaffold and/or of its substituents modulate the dynamics of the photoisomerization. All the indications coming from our computations are in line with and provide an explanation to the available experimental results.

1. Introduction

In the past decades the continuous progress in ultrafast laser technology has allowed the rise of a new fascinating research field named femtochemistry,^{1,2} devoted to the understanding and, more recently, to the control of the elementary excited-state reactive chemical processes.³ An ultrafast pump pulse prepares the excited molecule in a coherent state, a matter wave packet, which explores the electronic surface in the nuclear coordinates space moving according to quantum mechanics. The complexity of the phenomena which can take place, due to the rich topologies of the molecular excited-state surfaces, requires both experimental and theoretical studies for their full understanding.² With the aim to get highly accurate results, most of the existing theoretical studies

on excited-state reactivity have been performed in the gas phase on relatively small model systems, in which the “photoactive moiety” is as small as possible. These kinds of studies have allowed a fundamental advance in the knowledge of the basic mechanisms and processes involved in the excited-state reactivity, just think for example about the clarification of the primary role played by conical intersections between electronic states in determining the fate of photochemical processes.⁴

Parallel studies are desirable to understand how these basic mechanisms and processes apply in relatively large molecules and how they are affected by the existence of bulky and/or aromatic substituents linked to the photoactive moiety, as it often happens in molecules of technological interest. While these studies have been traditionally tackled from a “physical” perspective, introducing a bath of intramolecular modes to simulate decoherence and dissipative effects,⁵ new computational technologies and the increased computer speed

* Corresponding author e-mail: f.santoro@ipcf.cnr.it.

[†] Istituto di Biostrutture e Biommagini del CNR.

[‡] Istituto per i Processi Chimico-Fisici del CNR.

are making feasible a more satisfactorily approach, which takes into account the chemical specificity of the substituents including them explicitly in the electronic calculations. In this spirit, for example, an increasing number of “on the fly” quantum or semiclassical dynamical studies has been appearing in the literature.⁶

The hope and the ultimate goal of studies on the chemical effects of substituents on photochemical processes is to contribute to the establishment of some general and transferable propensity rules which allow the “factive” knowledge the chemists look for, enabling them to predict and, at the occurrence, to alter the dynamics and the fate of the process of interest. In this paper we deal with photoisomerization processes through twisting around a double bond. These reactions are widely studied for their biological and technological interest both in prototype molecules as ethylene and stilbene⁷ and in molecules more directly involved in biological processes as retinal⁸ or in important technological applications as cyanines.^{9–11}

Besides exhibiting intriguing properties in their aggregated form,^{12,13} cyanines, due their photophysical behavior, can be considered a prototypical case of study.^{14–29} A trans–cis isomerization around one of the CC bonds of the polymethine chain is involved in the $S_1 \rightarrow S_0$ deactivation process.^{25,26} This feature explains why cyanines exhibit rather short excited-state lifetime and a low fluorescence quantum yield,^{19–22} unless they are dissolved in very viscous solvents²⁷ or adsorbed on surfaces.²³ The effectiveness of the deactivation depends on general and basic physicochemical effects, such as the initial driving force to the twisting, the existence of a minimum on the excited surface, the location of the conical intersection relative to the minimum, the necessity for an IVR (intramolecular vibrational redistribution) during the dynamics, that are operative in several classes of compounds. This increases the general interest of understanding the factors that modulate the trans–cis isomerization, the deactivation mechanisms, and the lifetime of the excited state of cyanines. Therefore here we report a quantum mechanical study of several cyanines, sketched in Figure 1. This paper, by means of a series of static calculations (dynamics simulation will be the object of a forthcoming study), is aimed to get a close picture of the cyanine excited-state behavior, tackling the following questions:

(i) Do the substituents on the photoactive moiety change the character of the electronic transitions? (ii) Do the eventual differences influence their excited-state dynamics? (iii) If the answer to the previous points is positive, how can the effect of the nature of the atoms of the fused rings and/or of its substituents be rationalized? (iv) What is the role played by steric hindrances? (v) To what extent the photophysical behavior is modulated by environmental effects? (vi) Do the substituents have an understandable effect also on the location and the energetic of the conical intersection?

In our study we selected 3,3'-diEt-2,2'-thiacyanine iodide (Et-TCY according to ref 14) as the reference compound, since in the literature can be found a good amount of data concerning its stationary and time-resolved absorption and fluorescence spectra^{14,15} and resonance Raman spectra.¹⁷ Furthermore it has been utilized in the first coherent control

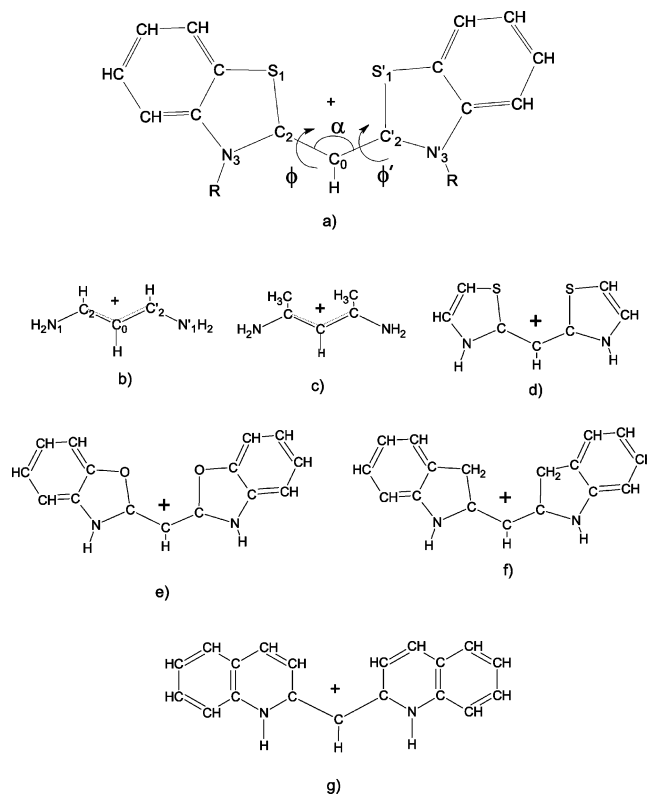


Figure 1. Schematic drawing of the different cyanine studied in the present paper: (a) Et-TCY (R = ethyl group) and H-TCY (R=H); (b) stCY; (c) CH₃-stCY; (d) H-TCY-sm; (e) OCY; (f) CH₂CY; (g) 2-Quino.

experiment of a photoisomerization process in the condensed phase,²² and an exploration of the S_1 reactive surface is necessary to get insights on the mechanism of the control induced by the shaped laser pulse.

To distinguish between conjugation and steric effects on the photoisomerization we also investigate a similar molecule (H-TCY, see Figure 1) in which ethyl groups are replaced by hydrogen atoms. Comparing Et-TCY and H-TCY with the simple stCY, with oxacyanine (OCY) and CH₂CY (two analogues of H-TCY in which the sulfur atoms are substituted by oxygen atoms and CH₂ groups, respectively), and with 2-Quino (in which the nitrogen atom is inserted in a six-member ring) will help to highlight the effect of fused aromatic ring and of their chemical nature.

Our study has been performed both in the gas phase and in methanol, through the inclusion of explicit solvent molecules and the adoption of polarizable continuum models.³⁰ This represents a significant improvement with respect to gas-phase models, allowing to take into proper account, and hence to investigate, the electrostatic effects of the solvent at least on the initial part of the excited electronic surface, i.e., on the driving force to the bond twisting.

From the methodological point of view, the theoretical study of the excited state reactivity, in the condensed phase, of molecules containing more than 40 atoms is not a trivial task, that can be difficultly tackled by using a single method. We have thus resorted to an integrated computational approach, in which several quantum mechanical methods have been cross-utilized in order to couple the computational

feasibility with the maximum of accuracy attainable at the moment for studying such large compounds. On the other hand, we resort to the conceptually simple but powerful traditional tools of the theoretical chemistry, such as molecular orbitals and population analysis, trying to infer general and transferable information on the driving forces of the photoisomerization reaction and on the physical-chemical effects that can influence it.

2. Computational Details

Due to the large size of the system under investigation, an extended use of the CASSCF/MP2 approach (utilized in ref 29) for the characterization of the stationary points on the S_1 surface and the minimum energy path is not feasible, we thus utilized different computational methods. Vertical transition energies have been calculated by Time-Dependent density functional (TD-DFT), employing the PBE0³¹ functional. Despite the absence of adjustable parameters, when employed in TD-DFT calculations, PBE0 (TD-PBE0) has already provided excitation spectra in very good agreement with the available experimental results.^{32,33} We have checked that an extension of the basis set beyond the 6-31+G(d,p) does not significantly change the computed spectra.

Geometry optimizations on the S_1 surface have been performed at the CIS/6-31G(d) level, refining the energies by single-point TD-PBE0/6-31+G(d,p) calculations.

The lowest-energy S_0/S_1 conical intersection (CI) in the isomerization path has been located by CASSCF/6-31G(d) and the method of Bearpark et al.³⁴ Unfortunately the inclusion of the full π -orbitals active space is computationally prohibitive for the system under investigation. We adopted SA-2-CAS(6,6), a state-averaged CASSCF with equal weights for S_0 and S_1 , with 6 electrons in 6 orbitals (6,6), the largest feasible active space for such a search. We checked the dynamical correlation effect by TD-DFT, which very recently³⁵ has been proven to be able to reproduce the CASPT2 results at CI points in a model of retinal, calculated with a full π -orbitals active space.

Bulk solvent effects on the ground and the excited states have been taken into account by means of the Polarizable Continuum Model (PCM).³⁰ In this model the molecule is embedded in a cavity surrounded by an infinite dielectric, with the dielectric constant of the solvent (for methanol we have used the value 32.64). The cavity of the solute is defined in terms of interlocking spheres centered on non-hydrogen atoms, whose radii are optimized according to the UAHF model.³⁶ PCM/TD-PBE0 calculations have been performed according to the procedure outlined in ref 37.

Atomic charges and Wiberg bond orders³⁸ have been calculated on the ground of the natural bond orbital (NBO) analysis.³⁹

All the calculations have been performed by using the Gaussian03 package.⁴⁰

3. Results

While important theoretical contributions have been given to the qualitative understanding of the cyanine's photoisomerization,²⁸ only one high-accuracy, full π -orbitals active space, CASSCF/MP2 extended theoretical investigation has

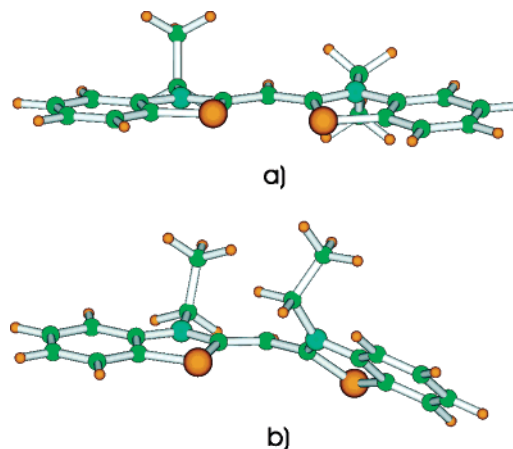


Figure 2. Schematic drawing of the PBE0/6-31G(d) S_0 geometry minima of Et-TCY: (a) trans minimum and (b) cis minimum.

been reported in the literature by Galvez et al.,²⁹ on the simple trimethine streptocyanine (stCY) reported in Figure 1, and on its five- and seven-unit polymethine analogues. As a first step of our analysis we have tested the computational approach described above on stCY. The comparison of our results with those of ref 29 (see Supporting Information for a detailed discussion) is comforting and supports the reliability of our calculations. The qualitative description of the S_1 PES obtained at the TD-PBE0/6-31G(d)/CIS/6-31G(d) level is very similar to that provided by CASMP2 calculation. Contrary to previous suggestion,²⁶ the initial relaxation of stCY on the S_1 PES is barrierless and can be described by a two-mode model, a skeletal stretching strongly coupled to a torsional deformation of the carbon framework, which leads toward a local C_2 minimum and then to the S_1 minimum, where the two amino groups exhibit a pseudoperpendicular arrangement. This minimum, corresponding to a Twist Intramolecular Charge Transfer (TICT), is slightly more stable than an adjacent S_1/S_0 conical intersection (CI) providing a path for the nonadiabatic evolution to S_0 , either to the trans or the cis minimum. From the quantitative point of view, the closest the system is to planarity the more accurate are the results of our approach, that instead underestimates the $S_1 - S_0$ gaps of the TICT pseudoperpendicular state, confirming the possible deficiencies of TD-DFT in describing charge-transfer transitions.^{41,42} As we will show below, the effect of the different substituents to the central trimethine moiety is already operative in the initial steps of the reaction, when the molecule is still close to planarity, and consequently their existence and nature is predicted to influence significantly the dynamics of the reaction.

3.1. Vertical $S_0 \rightarrow S_1$ Electronic Transition. Figures 2 and 3 show the trans and cis equilibrium structures of Et-TCY (Et-TCY and Et-TCY^{cis}) and H-TCY (H-TCY and H-TCY^{cis}), respectively, and Tables 1 and 2 report their main geometrical parameters optimized at the PBE0/6-31G(d) level of theory. Trans and cis isomers are defined with reference to the dihedral $N'_3-C'_2-C_0-C_2 = \phi'$ (see Figure 1 for atom labeling). Both for H-TCY and Et-TCY the two moieties bonded to the central carbon atom C_0 are identical. At

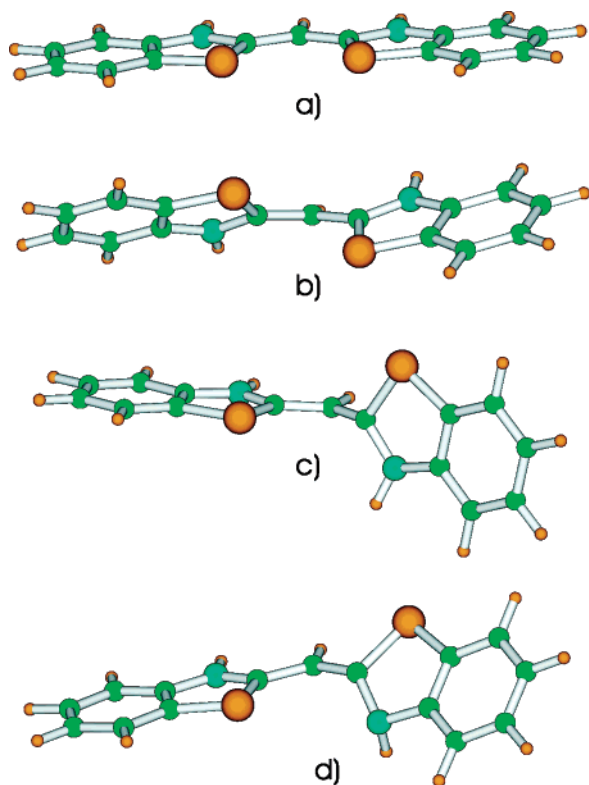


Figure 3. Schematic drawing of the different points on the S_1 PES of H-TCY: (a) FC; (b) S_1 -Min C_2 ; (c) S_1 -Min; and (d) CI.

Table 1. Main Geometrical Parameters of the Equilibrium S_0 Structures of Et-TCY and of the Two Minima on the S_1 Surface^e

	S_0 -trans ^a	S_1 -Min C_2 ^b	S_1 -Min ^b	S_0 -cis ^a
S_1-C_2	1.742	1.740	1.719	1.748
C_2-N_3	1.358	1.369	1.330	1.359
N_3-C_4	1.395	1.374	1.394	1.397
C_4-C_9	1.398	1.398	1.389	1.399
C_2-C_0	1.397	1.403	1.414	1.393
$S'_1-C'_2$	1.742	1.740	1.759	1.740
$C'_2-N'_3$	1.358	1.369	1.390	1.351
$N'_3-C'_4$	1.395	1.374	1.389	1.401
$C'_4-C'_9$	1.398	1.398	1.390	1.399
$C'_2-C'_0$	1.397	1.403	1.429	1.409
$S_1-C_2-C_0$	125.5	122.9	119.3	124.5
$S'_1-C'_2-C'_0$	125.5	122.9	117.9	119.3
$C_2-C_0-C'_2$	127.6	123.4	120.5	127.9
ΩC_2^c	360.0	360.0	351.6	360.0
ΩN_3^c	360.0	360.0	359.2	360.0
ϕ^d	176.1	153.0	177.3	179.5
ϕ'^d	176.1	153.0	114.8	41.7

^a Computed at PBE0/6-31G(d) level of theory. ^b Computed at CIS/6-31G(d) level of theory. ^c Sum of the bond angles with vertex at the indicated nucleus. ^d $\phi = N_3-C_2-C_0-C'_2$, $\phi' = N'_3-C'_2-C'_0-C_2$. ^e Distances in angstroms, angles in degrees.

variance with H-TCY, Et-TCY shows a small deviation from planarity (ϕ and ϕ' dihedral angles in Figure 1 are $\approx 176^\circ$), allowing for the decrease in the steric hindrance between the ethyl substituents at N_3 and N'_3 . This result is in agreement with experiments¹⁴ which reports an angle between the two rings smaller than 15° ($\approx 8^\circ$ according to our

calculations). The other geometrical parameters are very similar in the trans isomers of the two molecules, confirming that the substitution of Et- with H- does not significantly alter their π electron system.

On the contrary, the equilibrium structures of H-TCY^{cis} and Et-TCY^{cis} are remarkably different, since Et-TCY^{cis} exhibits a significant deviation from the planarity, with one ring about coplanar to the central C_0-H bond and the other rotated ($\phi' \approx 42^\circ$) so as to decrease the steric repulsion between the ethyl substituents (see Figure 2). This effect is by far reduced when Et- is substituted by H-, and H-TCY^{cis} can keep a pseudoplanar structure ($\phi' = 5^\circ$), allowing a more effective π -electrons delocalization.

In Table 3 are collected the computed energies of the $S_0 \rightarrow S_1$ electronic transition for the trans and cis isomer of Et-TCY and H-TCY.

TD-PBE0 computations predict a strong absorption band located at ≈ 3.4 eV for Et-TCY and ≈ 3.2 eV for Et-TCY^{cis}. Those values are within 0.5 eV of their experimental counterpart (obtained in methanol solution), and the agreement is within 0.36 eV when solvent effect is taken into account by means of the PCM method (vide infra). This good result witnesses that TCY is a more favorable case for TD-DFT than the unsubstituted stCY (see Supporting Information).

When considering the relative behavior of cis and trans isomers of Et-TCY, TD-PBE0 results show a perfect agreement with experiments. In fact, $S_0 \rightarrow S_1$ transition in Et-TCY is predicted more intense and blue-shifted (by 0.18 and 0.17 eV according to calculations and experiments, respectively) with respect to Et-TCY^{cis}. Such a large difference is mainly due to the different degree of planarity of the two isomers, as testified by the much smaller difference found between the two isomers of H-TCY, both planar. These results show that TD-PBE0 calculations are able to reproduce the effect of deviation from the planarity on the absorption spectra of Et-TCY and H-TCY.

Apart from the differences mentioned above, the behavior of the excited states of H-TCY and Et-TCY is very similar. For both compounds, the $S_0 \rightarrow S_1$ transition has a predominant HOMO \rightarrow LUMO character. Considering the central allyl moiety, the HOMO is mainly localized on the C_0 atom (see Figure 4), as a "classical" bonding HOMO orbital of an allyl group (see Figure 5), whereas the LUMO has a nodal plane on C_0 , and its density is moved on the two "external" atoms (C_2 and C'_2) of the allyl moiety. LUMO has also an antibonding character with respect to the C_2-S_1 and C_2-N_3 bonds, and benzenic rings remarkably contribute both to the HOMO and the LUMO. Considering the trans isomer, a natural bond order analysis (NBO) (at HF and CIS level of theory) confirms that both in S_0 and S_1 the electronic density is symmetric on the two side-moieties and most of the positive charge is carried by the 5-atoms rings adjacent to the central C_0 atom (which in S_0 is partially negatively charged) and in particular by their sulfur nuclei (whose charges are $\approx +0.5$ au in both the states), revealing their important electron-donor function in thiacyanines. Upon the $S_0 \rightarrow S_1$ transition there is a net transfer from the central C_0

Table 2. Main Geometrical Parameters of the Equilibrium S_0 Structures of H-TCY and Some Important Points on the S_1 Surface^f

	S_0 -trans ^a	S_1 -180 ^b	S_1 -MinC ₂ ^b	S_1 -135 ^b	S_1 -Min ^b	CI-CAS ^c	S_0 -cis ^a
S ₁ -C ₂	1.740	1.744	1.739	1.721	1.714	1.697	1.744
C ₂ -N ₃	1.352	1.371	1.365	1.334	1.327	1.311	1.352
N ₃ -C ₄	1.387	1.359	1.367	1.383	1.385	1.390	1.387
C ₄ -C ₉	1.398	1.400	1.398	1.390	1.388	1.386	1.398
C ₂ -C ₀	1.392	1.395	1.399	1.397	1.411	1.446	1.389
S ₁ '-C ₂ '	1.740	1.744	1.739	1.760	1.758	1.788	1.739
C ₂ '-N ₃ '	1.352	1.371	1.365	1.383	1.391	1.426	1.349
N ₃ '-C ₄ '	1.387	1.359	1.367	1.381	1.389	1.428	1.391
C ₄ '-C ₉ '	1.398	1.400	1.398	1.389	1.386	1.370	1.398
C ₂ '-C ₀ '	1.392	1.395	1.399	1.436	1.425	1.461	1.396
S ₁ -C ₂ -C ₀	127.3	128.6	125.6	122.5	122.8	123.2	127.2
S ₁ '-C ₂ '-C ₀ '	127.3	128.6	125.6	117.6	119.9	118.0	121.0
C ₂ -C ₀ -C ₂ '	127.4	130.6	124.5	120.5	121.4	120.2	127.9
Ω C ₂ ^d	360.0	360.0	360.0	348.0	351.2	346.6	360.0
Ω N ₃ ^d	360.0	360.0	359.8	356.6	354.1	334.5	360.0
ϕ ^e	180.0	180.0	155.4	171.0	178.5	180.5	176.7
ϕ' ^e	180.0	180.0	155.4	135.0	111.7	109.2	5.3

^a Computed at PBE0/6-31G(d) level of theory. ^b Computed at CIS/6-31G(d) level of theory. ^c Computed at SA-2-CAS(6,6)/6-31G(d) level of theory. ^d Sum of the bond angles with vertex at the indicated nucleus. ^e ϕ = N₃-C₂-C₀-C₂', ϕ' = N₃'-C₂'-C₀-C₂'. ^f Distances in angstroms, angles in degrees.

Table 3. Vertical Excitation Energy (in eV) for the Cis and Trans Isomers of Et-TCY and H-TCY: TD-PBE0/6-31+G(d,p)//PBE0/6-31G(d) Calculations^d

Et-TCY					
trans			cis		
gas phase	solution	exp ^c	gas phase	solution	exp ^c
3.37(1.01)	3.29(1.19)	2.93	3.18(0.81)	3.11(0.97)	2.76
H-TCY					
trans			cis		
gas phase	solution ^a		gas phase	solution ^a	
3.42(1.08)	3.35(1.29)		3.36(1.07)	3.29(1.27)	
	3.34(1.29) ^b			3.28(1.28) ^b	

^a PCM calculations. ^b Geometry optimized in methanol solution by the PCM method. ^c From ref 14. ^d Oscillator strengths are given in parentheses.

to the side rings. In particular the density lost by C₀ moves to the adjacent C₂/C₂' centers.

Electron density of Et-TCY^{cis} is instead partially asymmetric, due to the strong nonplanarity of its equilibrium geometry. In S_0 the positive charge is slightly more localized (by ≈ 0.1 au) on the rotated ring (hereafter labeled as right), since the HOMO is slightly more localized on the planar moiety (left ring + C₀ atom). *Therefore in the case of Et-TCY^{cis} the $S_0 \rightarrow S_1$ transition has a weak character of charge transfer* (approximately 0.2 au from the planar to the rotated moiety). Nevertheless, this fact does not affect the reliability of our TD-PBE0 calculations, as shown by the nice comparison with the experimental vertical excitation energies (vide supra). The charge transfer character is remarkably smaller in H-TCY^{cis}, whose structure is much less asymmetric.

In both isomers, the more “delocalized” character of the LUMO can explain why S_1 has a slightly larger dipole moment than S_0 (≈ 4.1 and 3.9 D, respectively, according to

CIS/6-31G(d) calculations in H-TCY) giving account of the red-shift predicted by PCM/TD-PBE0 calculations in methanol solution.

We have further examined the solvent effect by performing a test geometry optimization on H-TCY in methanol, finding that, due to the remarkable rigidity of the fused aromatic rings, the solvent has a negligible effect on the equilibrium geometries. In fact the vertical excitation energy changes indeed by only ≈ -0.007 eV when the geometry optimized in solution is used.

The possible effect on the absorption spectra of the formation of explicit interactions with methanol solvent molecules has been tested optimizing the coordination of two methanol molecules to H-TCY at the PBE0/6-31G(d) level. It is predicted the formation of hydrogen bonds between the NH groups (partially positively charged) and the oxygen atom of methanol, with a coordination energy to H-TCY ≈ 7 kcal/mol more exoergic than a hydrogen bond between two solvent molecules (PCM/PBE0/6-31+G(d,p) calculations in methanol solution). However the two methanol molecules do not significantly affect the absorption spectra (red-shift of ≈ 0.001 eV). Furthermore, the ethyl substituents in Et-TCY are expected to weaken the coordination of methanol molecules, so that explicit solute–solvent interactions can be neglected when considering the optical properties of cyanine.

In summary, TD-PBE0 predictions on the vertical absorption maxima of cis and trans isomers of Et-TCY, and, especially, on their difference, are in good agreement with experiments, supporting the reliability of our computational approach for the study of cis–trans isomerization on S_1 surface. Furthermore, H-TCY is a good model for Et-TCY, mostly when the characteristic and the dynamics of the trans isomer are taken into account. Solvent effect on the equilibrium structure is negligible so that in the following we always consider geometries optimized in the gas phase.

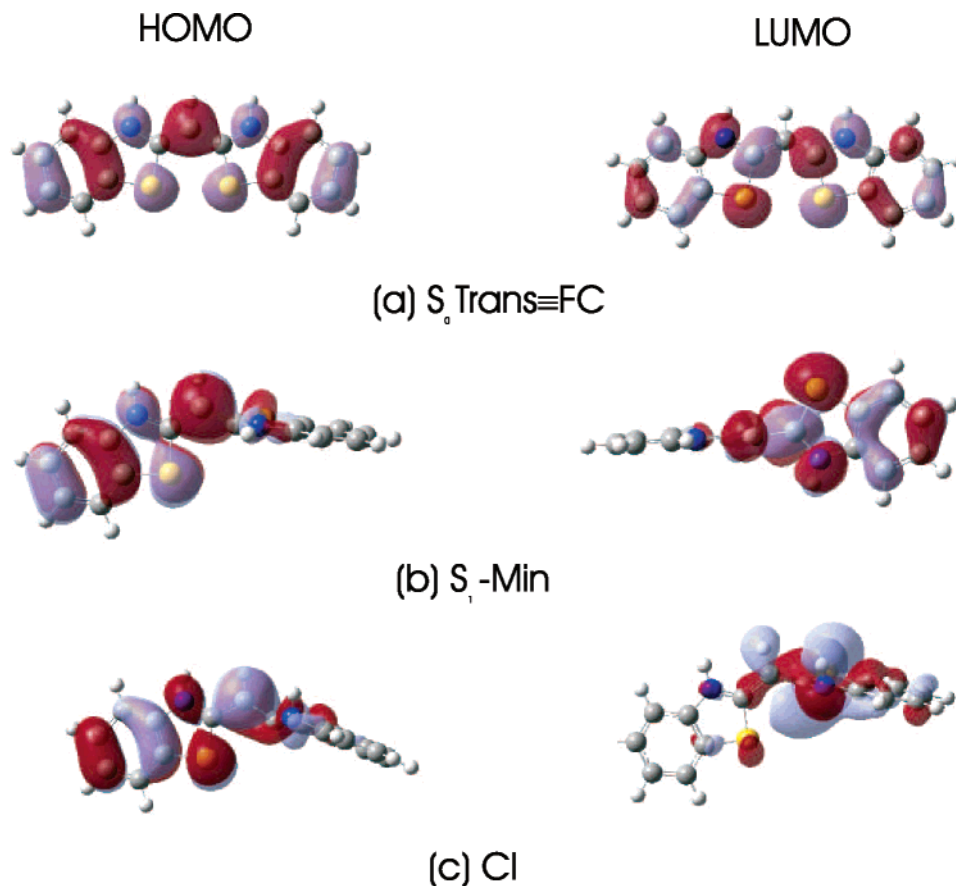


Figure 4. Schematic drawing of the HOMO and the LUMO of H-TCY, at **FC** (a), **S_1 -Min** (b), and **CI** (c), computed at PBE0/6-31G(d) level. Notice that at TD-PBE0 level the description of the transition is only slightly improved by changing the basis set from 6-31G(d) to 6-31+G(d,p); this also means that the shape of the more involved orbitals, computed by the two different basis sets, is the same.

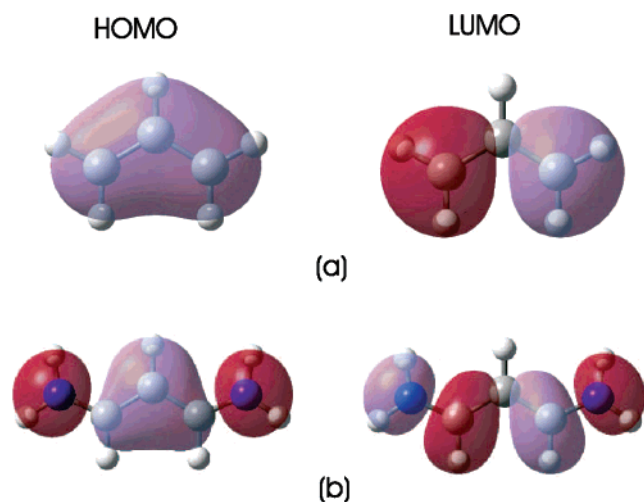


Figure 5. Schematic drawing of the HOMO and the LUMO of (a) an allyl group and (b) stCY, computed at PBE0/6-31G(d) level.

3.2. Stationary Points on the S_1 PES. Minima on S_1 have been computed both for H-TCY and Et-TCY, and their structures are very similar in the two molecules, as can be seen from Tables 1 and 2. As a consequence, the time-consuming optimization of the S_0/S_1 conical intersection has been performed only for the smaller H-TCY. If not stated differently, in the following we discuss the results for H-TCY.

Starting from the Franck–Condon (**FC**) structure CIS/6-31G(d) geometry optimization predicts the existence of a shallow minimum for $\phi = \phi' \approx 155^\circ$ (see Figure 3b), confirmed by a calculation of the Hessian matrix. The two rings keep an equivalent structure in this minimum (hereafter **S_1 -Min C_2**) exhibiting a C_2 symmetry. The most relevant geometry changes with respect to the S_0 trans minimum (hereafter **S_0 -trans=FC**) concern the elongation of the C_2 – N_3 bonds and a shortening of the N_3 – C_4 ones. The above results can be explained by the inspection of Figure 4: the HOMO is nonbonding on C_2 – N_3 and antibonding on N_3 – C_4 , while the opposite occurs for the LUMO. The charge distribution of the S_0 and S_1 states of H-TCY at **S_1 -Min C_2** is very similar to the ones computed at **S_0 -trans**, confirming that no significant change occurs in these states till the symmetry is preserved.

CIS geometry optimizations predict also the existence of a strongly asymmetric absolute minimum (**S_1 -Min**) where $\phi' \approx 112^\circ$, confirmed also through a calculation of the Hessian matrix. In **S_1 -Min** the two rings are no more equivalent, ϕ is $\approx 180^\circ$ and the “left” ring of Figure 3c is coplanar with the central C_0 –H bond. Furthermore, N_2 – C_3 and C_2 – S_1 are considerably shorter than in **S_0 -trans**, while the opposite occurs for N'_2 – C'_3 and C'_2 – S'_1 . These features can be rationalized by comparing the frontier orbitals of **S_0 -trans** and **S_1 -Min** reported in Figure 4. In **S_1 -Min** the HOMO

orbital is totally localized on the left ring and the central C_0 atom, while the LUMO is localized on the right ring. At S_1 -Min, according to TD-PBE0, $S_0 \rightarrow S_1$ is mainly a HOMO \rightarrow LUMO transition and can therefore be described as an intramolecular charge transfer, confirming previous computational results on the small stCY.²⁹ Going from S_0 -trans to S_1 -Min on the S_1 surface, the left ring loses the LUMO strong antibonding interactions on N_2-C_3 and C_2-S_1 thus inducing their shortening. The opposite geometry changes occur on the right ring, since here the $N'_2-C'_3$ and $C'_2-S'_1$ antibonding character of the LUMO is stronger at S_1 -Min than at S_0 -trans.

The TICT nature of the $S_0 \rightarrow S_1$ is confirmed by a NBO population analysis on S_0 and S_1 (at HF and CIS level of theory, respectively), showing that in S_0 the positive charge is almost totally localized on the right ring (+0.85 au) and in particular on the 5-atoms ring (0.64 au), while in S_1 the right ring is almost neutral (+0.15 au). It is interesting to notice that within the planar moiety (left ring + C_0-H), the most evident density change takes place on the central C_0-H (strongly contributing to the HOMO), whose charge increases by $\approx +0.5$ au following $S_0 \rightarrow S_1$ transition.

3.3. S_1/S_0 Conical Intersection. The main geometrical parameters of the SA-2-CAS(6,6) S_1/S_0 conical intersection (CI) are reported in Table 2, and its structure is depicted in Figure 3d. A calculation with a far larger active space SA-2-CAS(12,12) confirms that at this geometry the two states are close to degeneracy (gap 0.1 eV). The reliability of the CI structure here determined is further supported by its close analogy with that accurately located in ref 29 in stCY. In fact the CI structure differs from the S_1 -Min for an asymmetric-skeletal motion (similar to the one driving S_1 -MinC₂ to S_1 -Min) and a marked pyramidalization of N'_3 which pushes the H atom out-of-the average left-ring plane. Both these motions play an important role in reaching the CI from S_1 -Min. The energy of S_0 increases more steeply along the pyramidalization while the energy of S_1 increases more steeply along the skeletal-stretching. At CI the TD-PBE0/6-31+G(d,p) calculation also predicts a very small $S_0 - S_1$ energy gap (0.27 eV), confirming that the S_1/S_0 conical intersection is reached from S_1 -Min mainly distorting its structure along the asymmetric stretching and the N'_3 pyramidalization. This conclusion is supported by a TD/PBE0 scan of the S_0 and S_1 surface as a function of the $H'-N'_3-C'_2-S'_1$ torsion and of an asymmetric collective coordinate interpolating the S_1 -Min and CI structure. There is a region around CI where S_0 and S_1 are nearly degenerate. The best TD-PBE0 estimate of the conical intersection ($S_1 - S_0$ energy gap = 0.04 eV and $E(S_1) = 3.08$ eV) slightly differentiates with respect to CI for a less pronounced pyramidalization at N'_3 and a more pronounced asymmetry of the two rings.

Pyramidalization at nitrogen or carbon centers are frequently involved in the occurrence of a S_1/S_0 conical intersection, see for example the case of ethylene,⁴³ stilbene,⁷ and stCY.²⁹ For H-TCY CI is reached from S_1 -Min by destabilizing strongly the S_0 state (≈ 1.5 eV) and weakly the S_1 one (≈ 0.5 eV). Both at S_1 -Min and at CI the $S_0 \rightarrow S_1$ transition is characterized by a charge transfer from the

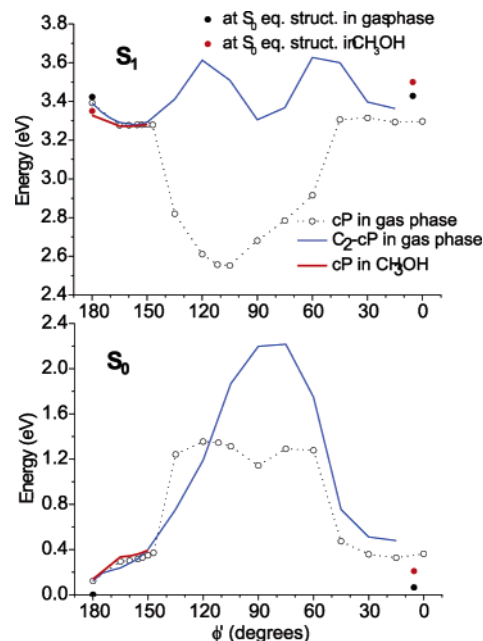


Figure 6. Energy of the lowest energy states as a function of the ϕ' dihedral for H-TCY. TD-PBE0/6-31G(d)//CIS/6-31G(d) calculations.

HOMO, fully localized on the left ring and the central C_0-H bond, to the LUMO on the right ring (see Figure 4). Further analysis shows that the pyramidalization strongly stabilizes the LUMO (by ≈ 0.9 eV), since as it appears in Figure 4, at CI the N'_3 lone pair can take part in an extended σ -bonding orbital. This effect partially compensates the S_1 energy destabilization due to geometry distortion from S_1 -Min to CI and, since it is only operative on S_1 (the LUMO is empty in S_0), it explains why the two electronic surfaces get close in energy, making feasible the occurrence of a conical intersection.

4. Reactive Paths on the S_1 Surface

In this section we study the possible paths on S_1 driving the system from the FC point ($\equiv S_0$ -trans) to the conical intersection.

4.1. From the FC Structure to the Perpendicular Minimum. One-Dimensional Path Analysis. To characterize the steps of the preferential path followed by the wave packet (WP) from FC to S_1 -Min we performed a relaxed PBE0/6-31+G(d,p)//CIS/6-31G(d) scan of the S_1 surface as a function of the ϕ' dihedral which is varied between 180° and 0° (see Figure 6).

The most significant structures of this constrained minima path (cP) are reported in Table 2. In the very initial dynamics at planar configurations (represented by S_1 -180 structure) the system enlarges the central $C_2-C_0-C'_2$ bond-angle (hereafter α) to decrease the $C_2-C'_2$ antibonding character of the LUMO. Rotating ϕ' the local minimum S_1 -MinC₂ is encountered. At the TD-PBE0 level it is closer to planarity ($\phi = \phi' \approx 165^\circ$) than it is at the CIS level, with an energy about 0.13 eV lower than the FC structure. The PBE0/6-31+G(d,p) computed fluorescence emission peak is ≈ 2.96 eV in the gas phase and ≈ 2.91 eV in methanol solution, i.e., with a Stokes shift of 0.46 and 0.44 eV, respectively

(for Et-TCY the same Stokes shifts are 0.48 and 0.46 eV, respectively).

Up to $\phi' = 150^\circ$ cP predicts that the molecule keeps approximately a C_2 arrangement with ϕ and ϕ' moving in a conrotatory way. In fact cP is practically isoenergetic to a path C_2 -cP (see Figure 6) in which the C_2 symmetry has been imposed, and therefore no significant driving force exists to lower the symmetry. On the contrary, upon further rotation of the ϕ' dihedral, a sudden and drastic geometry asymmetrization occurs accompanied by a corresponding remarkable stabilization of the S_1 state. That process is almost accomplished at $\phi' = 135^\circ$, whose geometry is strongly asymmetric (S_1 -135 in Table 2), and whose energy is about 0.5 eV lower than at $\phi' = 150^\circ$. Our computations thus predict the existence of an energy maximum on cP curve for $\phi' \approx 150^\circ$. The estimated energy barrier in H-TCY is very small, only $\approx 30 \text{ cm}^{-1}$ at TD-PBE0/6-31+G(d,p) level in gas phase. However, it is significantly higher $\approx 120 \text{ cm}^{-1}$ in Et-TCY, probably due to the larger steric hindrances of the two Et-groups and could influence the dynamics on the S_1 surface, increasing the S_1 -Min C_2 lifetime.

After S_1 -135, significant but minor skeletal rearrangements drive the system to the S_1 -Min structure, where TD-PBE0/6-31+G(d,p) predicts a $S_1 - S_0$ energy gap of 1.21 eV for H-TCY and 1.40 for Et-TCY. These values are probably underestimated for the known deficiencies of TD-DFT in reproducing charge-transfer transition-energies.^{41,42} A SA-2-CAS(6,6)/6-31G(d) computation for H-TCY predicts a value of 1.31 eV (to be compared with 1.18 eV obtained by TD-PBE0 with the same basis set), and this value increases to 1.38 eV if a much larger active space is used (SA-2-CAS(12,12)). This value is still probably underestimated by about 0.8 eV as one can roughly estimate from the results in ref 29 (see also Supporting Information) showing that for stCY the $S_1 - S_0$ CAS energy gap at S_1 -Min is $\approx 65\%$ of the CASMP2 value.

The motion along the cP from $\phi' = 150^\circ$ to S_1 -Min involves a different (asymmetric) skeletal motion with respect to the symmetric one along which the system moves from S_1 -180 to S_1 -Min C_2 ; in the same way the conrotatory motion of the two dihedral angles ϕ and ϕ' becomes disrotatory, and the left ring reassumes a planar arrangement with the C_0 -H ($\phi \rightarrow 180^\circ$). The necessity to acquire the right momenta along these modes can require some time, slowing down the reaction beyond what is done by the barrier along the cP.

Figure 6 shows that further rotating ϕ' beyond the S_1 -Min C_2 structure the C_2 -cP shows two other minima: the first at $\phi' \approx 90^\circ$, the other corresponding to a double-cis isomer. On S_0 this latter is slightly nonplanar in H-TCY ($\phi = \phi' = 14^\circ$), and it is 0.23 eV less stable than the trans isomer; in Et-TCY it is still less planar $\phi = \phi' = 28^\circ$ and less stable (0.46 eV) with respect to the trans isomer, due to the Et-groups effect. Anyway, Figure 6 shows that the high barrier makes the double-cis region inaccessible from FC, so that it can be ignored for the scopes of the present work.

Solvent Effect. Inspection of Figure 6 shows that including the solvent effect by means of the PCM method does not remarkably affect the first (C_2) part of cP but for an almost

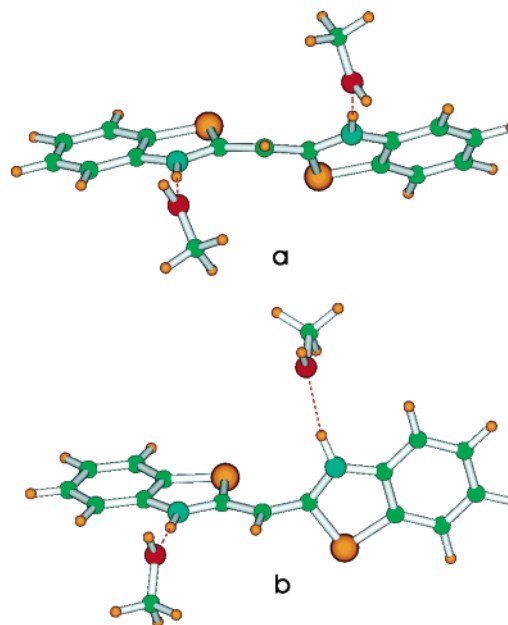


Figure 7. Schematic drawing of the adduct on the S_1 surface between H-TCY and two methanol molecules: (a) S_1 -Min C_2 and (b) S_1 -Min.

uniform stabilization of the S_1 state. It is not possible at the moment to give a reliable quantitative estimate of solvent effect on the TICT process, i.e., when the two moieties become strongly asymmetric. From the physical point of view, the nonequilibrium solvation effect should disfavor sudden electronic density change, since there is a slower component of solvent polarization that cannot be equilibrated to the solute. On the other hand, a polar solvent could favor charge localization. However, CIS/6-31G(d) calculations show that the dipole moment of the S_1 state does not dramatically increase when going from S_1 -Min C_2 to S_1 -Min (see Figure S2 in the Supporting Information), even if the latter exhibits a much larger charge asymmetry, as testified by a dipole moment oriented along the *long* molecular axis.

As a matter of fact, also pseudoplanar arrangements of the cyanine rings, though characterized by a symmetric charge distribution, exhibit a large dipole moment oriented along the *short* molecular axis, due to the presence of two parallel strong $S_1^+ - N_3^-$ local dipoles. This effect is lost for pseudoperpendicular geometry, as in S_1 -Min. Looking for a qualitative estimate of static solvent effect on the isomerization, we have calculated electrostatic solute-solvent interactions in the framework of PCM model, by using the excited-state atomic charges computed in methanol solution at the PCM/CIS/6-31G(d) level, according to the Merz-Kolmann⁴⁴ population analysis. The results of our model calculations (see Figure S2 in the Supporting Information) show that the presence of a polar solvent should favor the TICT S_1 -Min state over S_1 -Min C_2 by only ≈ 0.15 eV.

To get insights on the role of explicit solute-solvent interactions, we have then optimized at the CIS/6-31G(d) level the coordination of two methanol molecules to S_1 -Min C_2 and S_1 -Min (see Figure 7). In the symmetric S_1 -Min C_2 both methanol molecules have a hydrogen bond distance with the NH group of 1.90 Å, while in S_1 -Min the

hydrogen bond coordination is strongly asymmetric, with the $\text{CH}_3\text{HO}\cdots\text{HN}_3$ and $\text{CH}_3\text{HO}\cdots\text{HN}'_3$ hydrogen bond distances of 1.84 and 2.01 Å, respectively. Due to the TICT process the S_1 positive charge is localized mainly on the “left” ring (vide supra), leading to a stronger hydrogen bond. On the other hand, when the hydrogen bond distance optimized for $S_1\text{-MinC}_2$ is imposed, the energy of the $2\text{CH}_3\text{OH}/S_1\text{-Min}$ rises by ≈ 0.01 eV only. Those results, together with those of the electrostatic model calculations and with the fact that ethyl substituent should make solute/solvent interactions less strong, suggest that static solvent effects do not significantly affect the isomerization process.

Unfortunately, our present treatment is not able to give a quantitative estimate of the influence of nonequilibrium effects on the dynamical motion on cP and on the height of the energy barrier between $S_1\text{-MinC}_2$ and $S_1\text{-Min}$. An “ad hoc” study of the different relaxation time of solvent and solute degrees of freedom would indeed be necessary. On the other hand, our finding that total dipole moment changes its orientation during the motion on the S_1 surface suggests that a solvent dynamical effect could play a non-negligible role in the isomerization process.

Two-Dimensional Analysis. In the region $180^\circ < \phi' < 150^\circ$ the cP curve is very flat, suggesting the existence of a plateau on the S_1 surface. In such a case, it is likely that the wave packet (WP) broadens and follows also other decay paths than the cP. To verify this hypothesis and gain a better picture of the dynamics, we computed some bidimensional (2D) maps of the S_1 surface at TD-PBE0/6-31G(d) level. To build up each map we consider two structures chemically important for the reaction, say P_1 and P_2 , and explore the part of the S_1 surface which connects them. Restricting the 3N-6 dimensional space to a 2D one is clearly arbitrary; the nature of the process under consideration suggests that an important coordinate is the torsion around ϕ' dihedral; the second “collective” coordinate x is defined imposing that all the other internal coordinates move in a synchronous way. Say b any of these internal coordinates, b_1 and b_2 its values at the reference structures P_1 and P_2 , where the collective coordinate x is fixed to values x_1 and x_2 , respectively, then at each value \bar{x} of x the corresponding value \bar{b} of b is computed by linear interpolation $\bar{b} = b_1 + (\bar{x} - x_1)(b_2 - b_1)/(x_2 - x_1)$.

The first scan, reported in Figure 8a, describes a C_2 motion connecting FC and $S_1\text{-MinC}_2$ (i.e., the ϕ and ϕ' dihedral angles are kept equal, and, moving the collective coordinate x^a , the C_2 symmetry is preserved). As expected by the cP calculation, there is not any significant barrier to the torsion. Moreover in the 2D map the conrotatory rotation of ϕ and ϕ' appears to be coupled with the symmetric skeletal rearrangement from the beginning of the motion, a feature that could not be appreciated by the simple inspection of cP. Figure 8a gives further support to the existence of a local minimum at $\phi' \approx 160^\circ$ also at the TD-PBE0 level (165° is the more accurate estimate in the previous section). For a larger deviation from planarity, the potential along this symmetric motion increases till a barrier at $\phi = \phi' \approx 120^\circ$, already seen in the $C_2\text{-cP}$ path (Figure 6) too high to be crossed by WP.

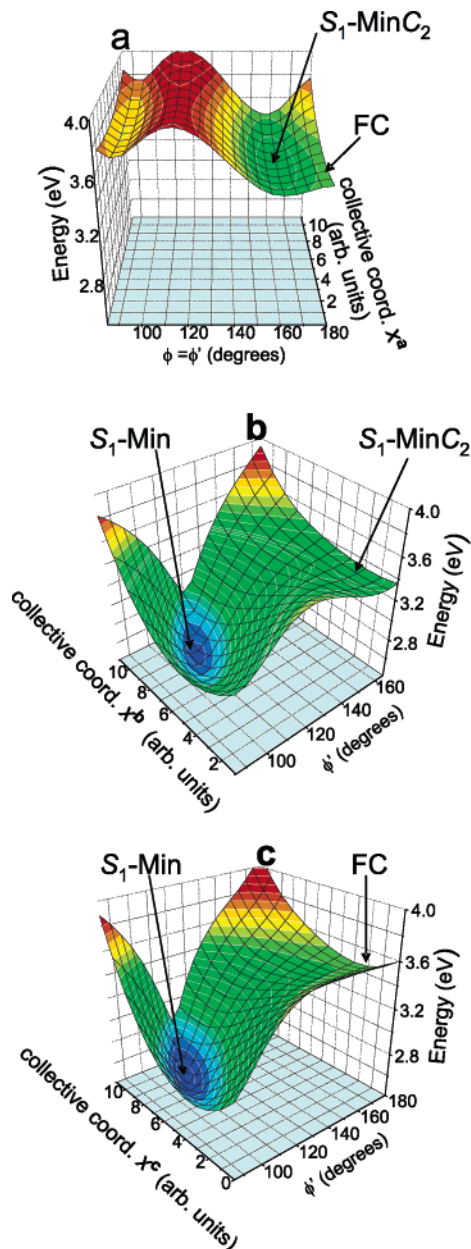


Figure 8. 2D maps of the S_1 surface as a function of the reactive ϕ' torsion and a collective coordinate x^p ($p = \text{a,b,c}$) obtained interpolating linearly (see the text) all the other coordinates between FC and $S_1\text{-MinC}_2$ (a), $S_1\text{-MinC}_2$ and $S_1\text{-Min}$ (b), FC and $S_1\text{-Min}$ (c). Notice that (a) is a C_2 map and hence $\phi' = \phi$.

Figure 8b reports a 2D surface connecting $S_1\text{-MinC}_2$ and the $S_1\text{-Min}$ structures; the first coordinate is the reactive ϕ' torsion, while the second collective coordinate x^b linearly interpolates the remaining internal coordinates, as explained above. As predicted by cP, the two structures are divided by a small barrier; the map additionally shows that the S_1 surface in the region of $S_1\text{-MinC}_2$ and of the barrier is considerably flat, bringing new information and suggesting that in this region WP spreads sensibly. Momenta orientation and intramolecular vibration redistribution (IVR) certainly plays a fundamental role at this stage on the time needed to cross the barrier, and a full dynamical study would be required.

Finally, to inquire the possibility that WP does not initially follow the cP path toward **S₁-MinC₂** moving instead in a direction that removes the C₂ symmetry from the beginning, we performed another 2D scan of the S₁ surface, choosing the ϕ' coordinate and the collective x^c obtained interpolating linearly all the other coordinates (including ϕ) between **FC** and **S₁-Min** (Figure 8c). There is a large initial plateau till about $\phi' = 150^\circ$, without any barrier to break the symmetry of the two rings. The 2D map therefore evidences the existence of an alternative path to cP for the isomerization which does not involve **S₁-MinC₂**. A quantitative estimate of its relative efficiency with respect to cP needs a full dynamical investigation. To get a very rough estimate we computed an average acceleration from **FC** to two structures at $\phi' = 165^\circ$, the first corresponding to the C₂ minimum at the TD-PBE0 level (**S₁-MinC₂[TD]**), the second (**S₁-165as**) corresponding to the minimum energy structure along the 2D map in Figure 8c. The time needed to reach **S₁-165as** is predicted to be comparable to the one needed to reach **S₁-MinC₂[TD]**. Even if the energy gain at **S₁-165as** is much lower, it is indeed geometrically closer to **FC** than **S₁-MinC₂[TD]** is, since this latter is more shifted along other coordinates.

5. Fluorescent State and Photoisomerization Dynamics

Fluorescence. The Et-TCY experimental fluorescence is peaked at ≈ 480 nm (2.58 eV),^{14,16} i.e., with a Stokes shift of ≈ 0.35 eV with respect to the absorption maximum. Our results strongly suggest that this fluorescence arises from the **S₁-MinC₂** intermediate. In fact, on one hand, its computed Stokes shift, 0.48 eV, is in good agreement with the experiments and, on the other hand, the alternative candidate **S₁-Min** has to be discarded since it is predicted to emit at far shorter frequencies (1.4 eV).

The lifetime of the Et-TCY fluorescence is expected to be on the picosecond time scale (an old experimental estimate¹⁵ reports a value of 1.7 ps). This feature supports our assignment of **S₁-MinC₂** as the fluorescent state. In fact a relatively long lifetime of **S₁-MinC₂** can be explained on the grounds of the following arguments: (a) S₁ is very flat in the **FC** region, and a small but not negligible barrier (about 120 cm⁻¹) separates the **S₁-MinC₂** intermediate from **S₁-Min**; (b) once reached **S₁-MinC₂** it is necessary to pump energies in asymmetric modes (disrotatory motion ϕ and $\phi' +$ asymmetric skeletal mode of the two rings) which are different from the initial C₂ motions driving **FC** to **S₁-MinC₂**; (c) the mass of the system and the presence of the solvent both slow the dynamics.

On the contrary, structures close to **S₁-Min** could be responsible for the low emission experimentally found when Et-TCY is adsorbed on aerosol-OT (AOT) surfactant (≈ 2.06 eV).¹³ This peak has been interpreted as coming from AOT₆/Et-TCY₆ aggregates, in which the Et-TCY molecules exhibit a twisted geometry, and our results support this interpretation. In fact, as we discussed in a previous section, even if TD-DFT results predict a much lower frequency for the emission from **S₁-Min** (≈ 1.4 eV in gas phase), CAS results on H-TCY and comparison with CAS/CASMP2 results for st-CY (see

Supporting Information) suggest that this value could be underestimated by about 0.8 eV. As expected for an ICT transition, the S₁ – S₀ oscillator strength at **S₁-Min** predicted by TD-PBE0 is very low (≈ 0.01). However, it must be noticed that also the experimental ICT band¹³ is very weak and that its intensity is increased by aggregation phenomena on the surface, which we cannot take into account by our calculations.

Photoisomerization Dynamics. Our results suggest that two steps can be individuated in the S₁ dynamics: (i) the motion from **FC** to **S₁-Min**, during which no S₁/S₀ non-radiative transition is possible due to their large energy gap (see Figure 6) and (ii) the motion from **S₁-Min** to **CI**. As discussed above, it is likely that the first step occurs along different paths, i.e., removing the C₂ symmetry from the beginning or passing through the **S₁-MinC₂** intermediate.

Up-conversion fluorescence of a cyanine similar to Et-TCY (where the Et-groups are substituted by sulfopropyl-groups), recorded at frequencies close to the maximum of the fluorescence steady spectrum, shows a biexponential decay, with a fast component on the subpicosecond scale and a slow component of ≈ 5 ps.⁴⁵ The former component is assigned to a motion on the excited surface out of the FC region, while the latter is assigned to the S₁ → S₀ transition. Analogous assignments have been proposed for the similar time dependence of fluorescence, excited-state absorption, and ground-state recovery in 1144-C cyanine.^{46,47} For this molecule it has been speculated⁴⁷ that the two-time decays is a sign of a multidimensional dynamics on S₁ and hence of the involvement of different dynamical paths.

Our results on Et-TCY are consistent with this picture and suggest that the two different time scales could be due to the parts of the wave packet which go directly from **FC** to **S₁-Min**, escaping quickly from the FC region, or pass by **S₁-MinC₂**, emitting for a longer time. A full dynamical study is planned to confirm this hypothesis.

For the case of 1144-C cyanine, different studies ascribe the rate-limiting step of the photoisomerization either to the initial bond twisting⁴⁸ (i.e. our step (i)) or to the nonadiabatic S₁ → S₀ transition⁴⁷ (i.e., the S₁ motion from the perpendicular minimum to the conical intersection, our step (ii)). Our results for Et-TCY indicate that both the two steps are likely to be important for the overall reaction rate. Step (i) is expected to be considerably slowed, beyond what is done by the existence of the barrier on S₁, also by dynamical factors as an inertia to the torsion, the solvent friction (which clearly influences the dynamics of 1144-C),^{46,47} and the necessity to pump energy on the right coordinates, at least for the path passing through **S₁-MinC₂**. In fact, during this minimum energy motion on S₁, it is required to transfer energies from symmetric to asymmetric modes, and this process likely requires a nonvanishing time to be accomplished.

On the other hand, also step (ii) is expected to require a substantial amount of time because of the predicted energy gap on S₁ between **CI** and **S₁-Min** which is (≈ 0.5 eV), even if this value is probably overestimated in our calculations since no TD-PBE0 optimization of the **CI** structure is possible. From the dynamical point of view, it is interesting to notice that **CI** is shifted with respect to **S₁-Min** along an

Table 4. NBO Population Analysis of the CIS/6-31G(d) Density Matrix of the Lowest Energy States for a Series of Different Carbocyanine (See Figure 1)

	atom-atom bond order				Wiberg bond order				extra diagonal Mulliken population	
	C ₀ –C ₂	N ₃ –C ₂	N ₃ –C ₄	C ₂ –X ₁	C ₀ –C ₂	N ₃ –C ₂	N ₃ –C ₄	C ₂ –X ₁	C ₀ –C ₂	C ₂ –C' ₂
S₀										
allyl	1.167				1.508				0.466	–0.036
stCY	1.135	1.089			1.397	1.391			0.534	–0.030
CH ₃ -stCY	1.133	1.081			1.366	1.351			0.540	–0.021
H-TCY	1.131	1.009	0.884	0.890	1.353	1.237	1.039	1.173	0.514	–0.016
H-TCY-sm	1.130	1.003	0.897	0.906	1.348	1.226	1.073	1.195	0.517	–0.020
OCY	1.125	1.028	0.862	0.889	1.333	1.237	1.023	1.065	0.543	–0.035
CH ₂ CY	1.144	1.043	0.843	0.865	1.377	1.302	0.994	1.015	0.545	–0.018
2-Quino	1.109	0.983		1.024	1.326	1.199		1.185	0.523	–0.028
S₁										
allyl	0.992				1.132				0.319	–0.104
stCY	1.039	1.028			1.191	1.283			0.427	–0.092
CH ₃ -stCY	1.036	1.024			1.163	1.252			0.415	–0.078
H-TCY	1.107	0.951	0.924	0.849	1.296	1.125	1.108	1.092	0.482	–0.051
H-TCY-sm	1.103	0.943	0.931	0.851	1.286	1.116	1.142	1.089	0.476	–0.057
OCY	1.100	0.971	0.904	0.846	1.279	1.131	1.096	0.990	0.514	–0.067
CH ₂ CY	1.115	0.981	0.896	0.859	1.311	1.172	1.086	1.013	0.516	–0.053
2-Quino	1.082	0.930		1.046	1.267	1.102		1.234	0.488	–0.046

^a Calculations relative to vertical excitation on the C₂ S₀ energy minimum optimized at the PBE0/6-31G(d) level.

asymmetric skeletal mode and a pyramidalization motion at N₃'. While it is clear that some time is necessary to populate the pyramidalization motion at N₃', the asymmetric motion driving S₁-Min to CI is similar to the one driving to S₁-Min, so that the wave packet arriving to S₁-Min should already have significant momentum along this coordinate.

6. Comparison with Different Cyanines

Effect of the Fused Rings: TCY vs stCY. The qualitative topology of the S₁ surface from FC to S₁-Min discussed above for x-TCY (x = Et- or H-) is similar to the one reported in the literature for stCY.²⁹ Nevertheless there are significant quantitative differences. In fact in stCY the initial relaxation path occurs along a steep path dominated by C₀–C₂ and C₀–C'₂ stretchings strongly coupled with torsional deformation around the above bonds, and the S₁-MinC₂ stationary structure (which is not a true minimum) already shows a pseudoperpendicular arrangement of the two side-chains. On the contrary for x-TCY, S₁-MinC₂ is only slightly nonplanar and is a true minimum separated by an energy barrier from S₁-Min.

Since the S₀ → S₁ transition has a predominant HOMO → LUMO character for both H-TCY and stCY and the shape of the frontier orbitals is qualitatively similar, how can we explain the significantly different shapes of the S₁ PES of H-TCY and stCY, with the consequent different dynamical behavior of the two molecules?

Analysis of the molecular orbitals can help rationalize these differences. Figure 4 shows that, due to the presence of the rings and of the sulfur substituents, the weight of the C₂/C'₂ atomic orbitals in the LUMO and the consequent C₂/C'₂ antibonding character is rather small, as testified by the small value of the extradiagonal negative Mulliken overlap population existing between those atoms (see Table 4). The

situation is different for stCY, where the contribution of the C₂/C'₂ atoms to the LUMO and their antibonding character are larger (see Figure 5), and indeed, the extradiagonal negative C₂/C'₂ S₁ Mulliken overlap population is almost double than in H-TCY. This results in a larger driving force to rotate the φ dihedral on S₁ for stCY, since a nonplanar arrangement of the two side-moieties decreases the C₂ – C'₂ antibonding character of the LUMO.

Significant differences are found in the HOMO as well. In stCY, C₂ and C'₂ noticeably contribute to the HOMO, that therefore has a substantial C₀/C₂ weight and C₀–C₂/C'₂ bonding character. As a consequence the S₀ → S₁ transition should be associated with a remarkable reduction of the C₀–C₂/C'₂ bond orders. In H-TCY and Et-TCY the contribution of C₂ and C'₂ to the LUMO is negligible and, thus, both HOMO and LUMO can be considered nonbonding orbitals with respect to the C₀–C₂/C'₂ bonds. On this ground it is not surprising that the increase of the lengths of these bonds associated with the S₀ → S₁ transition is very small (see Tables 1 and 2).

To put all the above considerations on a more quantitative basis, we resorted to natural bond order (NBO)³⁹ and Wiberg bond order (WBO) analysis.³⁸ The inspection of Table 4 shows that the S₀ → S₁ transition leads the C₀–C₂ bond order to decrease by ≈15% for stCY and only by ≈4% for H-TCY. Similar indications are provided by the overlap-weighted bond order based on the NBO analysis.

Analyzing the variation in the bond orders and in the equilibrium geometry suggests that, following S₀ → S₁ transition, the initial dynamics should involve the C₂–C₀–C'₂ bending and the C₂–S₁, C₂–N₃, and N₃–C₄ stretching motions (together with the symmetric ones on the right ring). The excitation of symmetric normal modes comprising these motions is probably responsible for the shoulder observed

on the absorption spectrum at ≈ 400 nm¹⁴ (i.e. ≈ 1300 – 1400 cm⁻¹ shifted with respect to the maximum) and the strong Raman bands¹⁷ at 1230 cm⁻¹ and at ≈ 1450 – 1500 cm⁻¹ (a group of bands).⁴⁹ A Raman spectrum of Et-TCY, computed at PBE0/6-31G(d) level, nicely reproduces these features showing a strong band at 1270 cm⁻¹ and a group of strong bands in the region 1500 – 1550 cm⁻¹ and confirms that they correspond to modes with strong contributions by the motions indicated above. On the other hand, as anticipated above, for stCY a larger involvement of the C₀–C₂ stretching modes is likely.

Shortly, for what concerns the C₂–C₀–C₂' moiety, while for stCY the $S_0 \rightarrow S_1$ transition has a predominant bonding/antibonding character, for H-TCY and Et-TCY it can be better described as nonbonding/nonbonding.

Both stCY and H-TCY show a S_1/S_0 conical intersection which is reached from **S₁-Min**, increasing the energies of both electronic states and moving along the asymmetric stretching and the pyramidalization at the nitrogen N₃' of the rotated moiety. Though the qualitative picture is similar, there is a substantial quantitative difference inasmuch that the **S₁-Min** and **CI** structures are much closer in stCY than in TCY, both from the energetic and the geometrical point of view. In fact in stCY the gap on the S_1 surface from **S₁-Min** to **CI** is just 0.05 eV at the CAS level, while it rises to about 0.5 eV for H-TCY at the TD-PBE0 level. Even if, as discussed above, this value is an upper limit, a significant increase of this energetic gap from stCY to H-TCY is expected, due to the cost to distort the fused ring. In particular, while at **S₁-Min** the hybridization of the N₃' atom is sp^2 (sum of the nitrogen valence bond angles 354°) in x-TCY, it is almost sp^3 in stCY (sum of the nitrogen valence bond angles 336°). Notice that the sp^2 hybridization of N₃' in x-TCY is not an artifact of the CIS optimization since this method correctly reproduces (apart from a slight underestimation) the N₃' hybridization in stCY (see Supporting Information). Therefore, we are dealing with a physical effect: when the ring π -system geometrical and electronic constraints are absent, N₃' pyramidalization is indeed much easier. These differences, together with those in the path from **FC** to **S₁-Min** reported above, suggest that the isomerization is much faster in stCY than in TCY.

Nature of the Fused Ring and of the Specific Heteroatom. Once verified that the presence of the fused rings deeply affects cyanine photoisomerization, it is interesting to investigate what is the effect of variations in their chemical structure. The presence of the methyl substituent on C₂/C₂' atoms in CH₃-stCY (see Figure 1) does not remarkably change the picture obtained for stCY (see Table 4).

This table also shows that, analogously, from the qualitative point of view, the behavior of the other fused ring cyanines (reported in Figure 1) is very similar to that of H-TCY. In particular, the bond order variation associated with the $S_0 \rightarrow S_1$ transition is quite limited as well as the C₂–C₂' antibonding character of the LUMO. Nevertheless, it is worthy to notice that when the sulfur atoms are substituted by oxygen atoms (oxacyanine, OCY) or CH₂ groups (CH₂CY) the C₀–C₂/C₂' bonds in the S_1 state are predicted to be slightly stronger, suggesting that for those

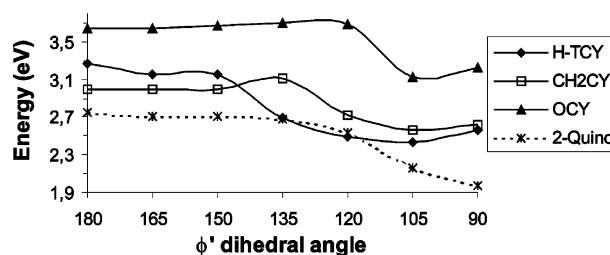


Figure 9. Energy of the S_1 state as a function of the ϕ' dihedral for four different cyanine molecules. TD-PBE0/6-31+G(d,p)//CIS/6-31G(d) calculations.

species the distortion from the planarity is less favored than in H-TCY. Figure 9, comparing the TD-PBE0/6-31+G(d,p)//CIS/6-31G(d) cP path for H-TCY, OCY, and CH₂CY, confirms this hypothesis. In fact also OCY and CH₂CY exhibit two minima on the S_1 surfaces: the first, rather shallow, at $\phi' \approx 180^\circ$, the second, the absolute minimum in the isomerization reaction path, with a pseudoperpendicular arrangement of the fused rings, corresponding to a TICT. Nevertheless, the energy barrier associated with the motion from the planar to the perpendicular minimum is remarkably larger, for OCY (≈ 500 cm⁻¹) and for CH₂CY (≈ 950 cm⁻¹) than for H-TCY, suggesting that for OCY and CH₂CY isomerization should be slower than for H-TCY and Et-TCY. This prediction nicely agrees with the experimental finding that the S_1 fluorescence lifetime for Et-OCY is longer than for Et-TCY (6.4 and 1.7 ps, respectively).¹⁵

A possible explanation of the lower barrier and the easier asymmetrization (which occurs at configurations closer to be planarity) in x-TCY is that the intramolecular charge-transfer process, and hence the asymmetrization of the molecule, can be assisted by the availability of the low-lying 3d orbital on the sulfur atoms for the formation of multiple bond with C₂ atoms.

Figure 9 reports also the cP curve of 2-Quino, which though being very flat up to 120° , does not exhibit any energy barrier before falling in the asymmetric TICT minimum at 90° . The larger steric hindrances of pyridine-like rings increases indeed the driving force to the torsion for 2-Quino, as testified by the fact that also the S_0 minimum energy geometry is not planar.

As a last remark we notice that a further support to the reliability of our calculations is the fact that the absorption maxima of OCY and of 2-Quino in methanol are predicted at 3.76 and 2.80 eV, respectively i.e., ≈ 0.4 eV blue-shifted and ≈ 0.55 red-shifted with respect to H-TCY. Those values are in very nice agreement with the experimental shift between Et-TCY, Et-OCY, and Et-2-Quino (0.33 eV and -0.57 eV, respectively).¹⁴

7. Discussion and Concluding Remarks

In this paper we have performed a thorough theoretical analysis of the S_1 excited-state surface of several $n = 0$ ¹⁴ cyanines, with a special focus on two of them, namely Et-TCY and H-TCY. The absorption and the fluorescence spectra computed in solution compare nicely with the available experimental results, supporting the reliability of our conclusions. Generally, the comparison with experimental

data for TCY, and with CASMP2 results for stCY,⁵¹ indicate that the computational methods adopted here give results quantitatively reliable for geometries close to planarity, while the TD-PBE0 S_1 energies must be considered affected by noticeable errors at strongly distorted geometries, where the $S_0 \rightarrow S_1$ transition has a clear charge transfer character. This would be a serious problem in detailed dynamical calculations, but, for the scopes of the present paper, the results presented still furnish a qualitatively correct description of the S_1 surface, as shown by the comparison with CASPM2 in the stCY case. The substituent effects here discussed are already operative for geometries close to planarity, where our results are reliable.

Due to their specific structure, cyanines show a rich dynamics with a competition between symmetric and asymmetric reactive paths and are a nice example of how the substituents can partially modify the nature itself of the optical transition, altering the initial driving force to the reaction.

Although the orbitals involved in the $S_0 \rightarrow S_1$ electronic transition are similar, the presence of the fused aromatic rings produces indeed some significant difference in x-TCY with respect to the model compound stCY. In x-TCY the $S_0 \rightarrow S_1$ transition is mainly nonbonding/nonbonding, and the S_1 surface around the FC region is rather flat with a scarce driving force to torsion. A shallow slightly nonplanar local minimum **S_1 -MinC₂** exists on the S_1 surface, separated by a small barrier (≈ 120 cm⁻¹) from the absolute asymmetrical minimum **S_1 -Min**, corresponding, as in stCY, to a TICT state.

Our results strongly suggest that **S_1 -MinC₂** is the state responsible for the Stokes-shifted fluorescence and for the $S_1 \rightarrow S_n$ transient absorption. Although a full dynamical study would be necessary to compute the lifetime of **S_1 -MinC₂**, the topology of the S_1 surface and the existence of the barrier are consistent with a picosecond(s) lifetime.

A barrier on the S_1 minimum energy path is predicted for several of the investigated cyanines (x-TCY, OCY, and CH₂CY), and it is suggested that a key factor determining its existence is the degree of planarity of the S_0 equilibrium geometry. When, due to steric hindrances, the S_0 minimum is already strongly twisted, S_1 PES could be barrierless (as in 2-Quino), and/or the FC excitation could occur in a region of the S_1 surface where the electronic effects responsible for the barrier are no more active. The existence of barriers on S_1 and hence local minima has been predicted⁵⁰ and is generally accepted in cases of carbocyanine ($n > 0$).

Concerning the possible isomerization path, our results suggest that the cP passing through the **S_1 -MinC₂** intermediate and other paths which remove the symmetry already in the FC region are probably competitive. This possible competition is enhanced by the scarce initial driving force to the torsion which is clearly lower in Et-TCY than in the smaller stCY. The exciting possibility that in Et-TCY the wave packet can follow simultaneously different paths toward the minimum **S_1 -Min** could play an important role in the coherent control of the Et-TCY photoisomerization which has been recently attained.²² In fact, the parts of the wave packet which reach **S_1 -Min** along these different paths could interfere depending on their relative phases, as in molecular

version of the Young double-slit interferential experiment, and this phenomenon would influence the later dynamics of the wave packet.

Apart from the insights on the dynamical behavior of Et-TCY, a synoptical analysis of the shape of the frontier orbitals of different cyanines not only explains the features depicted above but also allows us to sketch which are the most important interactions modulating the planarity of the cyanine moiety: (i) the C₂-C₀-C'₂ bonding character of the HOMO, favoring a planar conformation of the allyl moiety, (ii) the C₂-C'₂ antibonding character of the LUMO resulting in a driving force to distortion from the planarity of the cyanine, which increases at the increase of the weight of those atoms in the LUMO, and (iii) steric repulsion between the substituents on C₂ and C'₂ atoms. The first two factors explain the different flatness with the respect the initial torsion around the ϕ' dihedral of the S_1 PES of x-TCY and of stCY. The larger steric hindrance of the ethyl substituents gives instead an account for the energy barrier higher in Et-TCY than in H-TCY. The inspection of the frontier orbitals also explains why the pyramidalization of the N₃ center is required to go from the S_1 minimum to the S_1/S_0 conical intersection.

The photophysical behavior of cyanine depends on the chemical structure of the fused aromatic ring as well. The peculiar electronic structure of sulfur atoms can explain why in x-TCY the energy barrier connecting **S_1 -MinC₂** and **S_1 -Min** is noticeably lower than in OCY and CH₂CY, in agreement with experimental indications.

Our results confirm for Et-TCY the general description of the photoisomerization reaction predicted by Galvez et al.²⁹ on stCY, but they also point out significant quantitative differences showing that ad hoc modifications, even small, of the molecular scaffold and/or of its substituents can be used to modulate the dynamical behavior of $n = 0$ cyanines, suggesting which physicochemical effects (either electronic or steric) to rely on in order to design cyanines with optimized excited-state properties.

As a last remark cyanine is a clear example where remarkable changes in the electronic structure along the path have a large purely dynamical effect on the reaction. In fact, in correspondence to the shift from a symmetric to an asymmetric electronic density distribution, there is a change in the nature itself of the nuclear modes involved in the motion. This effect is likely to slow the reaction dynamics, even if the surface does not exhibit any significant energy barrier, since an energy redistribution is necessary to proceed along the reactive path. Of course also the solvent is sensible to a sudden change in the solute electronic density so that, beyond what is done by frictional effects depending on the shape of the twisting moiety, also solvent nonequilibrium effects are expected to contribute to slow the reaction rate.

Acknowledgment. The authors thank G. Krampert, P. Niklaus, G. Vogt, and G. Gerber of the Universität Würzburg who stimulated this study for many valuable discussions. F.S. acknowledges the hospitality of the Physikalisches Institut, Universität Würzburg (Germany) and the support of the European Community through the COCOMO Network.

Supporting Information Available: Detailed comparison of the performance on stCY of TD-PBE0//CASSCF and TD-PBE0//CIS methods utilized in this paper with respect to CASMP2//CASSCF of ref 29, excited-state dipole moment and solvation energy, and tables with the Cartesian geometries of the main structures of H-TCY and Et-TCY discussed in the text. This material is available free of charge via the Internet at <http://pubs.acs.org>.

References

- (1) Zewail A. H. *Femtochemistry: Ultrafast Dynamics of the Chemical Bond*; World Scientific Publishing Co. Pte. Ltd.: 1994; Vol. I and II.
- (2) *Femtochemistry and Femtobiology*; Douhal, A., Santamaria, J., Eds.; World Scientific Publishing Co. Pte. Ltd.: 2002.
- (3) (a) Judson R. S.; Rabitz H. *Phys. Rev. Lett.* **1992**, *68*, 1500. (b) Assion A.; Baumert T.; Bergt M.; Brixner T.; Kiefer B.; Seyfried W.; Strehle M.; Gerber G. *Science* **1998**, *282*, 918. (c) Shapiro M.; Brumer P. *Principles of the Quantum Control of Molecular Processes*; J. Wiley & Sons Inc.: 2003.
- (4) *Conical Intersections: Electronic Structure, Dynamics & Spectroscopy*; Domcke, W., Yarkony, D. R., Köppel, H., Eds.; World Scientific Publishing Co. Pte. Ltd.: 2004.
- (5) Domcke, W.; Stock, G. *Adv. Chem. Phys.* **1997**, *100*, 1.
- (6) (a) Ciminelli, C.; Granucci, G.; Persico, M. *Chem. Eur. J.* **2004**, *10*, 2327. (b) Weigart, O.; Migani, A.; Olivucci, M.; Robb, M. A.; Buss, V.; Hunt, P. J. *Phys. Chem. A* **2004**, *108*, 4685. (c) Ko, C.; Levine, B.; Toniolo, A.; Manohar, L.; Olsen, S.; Werner, H.-J.; Martinez, T. J. *J. Am. Chem. Soc.* **2003**, *125*, 12710.
- (7) Quenneville, J.; Martínez, T. J. *J. Phys. Chem. A* **2003**, *107*, 10076, see also references therein.
- (8) González-Luque, R.; Garavelli, M.; Bernardi, F.; Merchán, M.; Robb, M. A.; Olivucci, M. *Proc. Natl. Acad. Sci. U.S.A.* **2000**, *97*, 9379, see also references therein.
- (9) (a) Fabian, J.; Nakazumi, H.; Matsuoka, M. *Chem. Rev.* **1992**, *92*, 1197. (b) Czerney, P.; Graness, G.; Birckner, E.; Vollmer, F.; Rettig W. *J. Photochem. Photobiol. A* **1995**, *89*, 31. (c) Kaliteevskaya, E. N.; Razumova, T. K.; Tarnovskii, A. N. *Opt. Spectrosc.* **1999**, *1*, 126.
- (10) (a) Naber, A.; Fischer, U. C.; Kirchner, S.; Dziomba, T.; Kollar, G.; Chi, L. F.; Fuchs, H. *J. Phys. Chem. B* **1999**, *103*, 2709. (b) Spitler, M. T.; Ehret, A.; Kietzmann, R.; Willig, F. *J. Phys. Chem. B* **1997**, *101*, 2552.
- (11) (a) Seifert, J. L.; Connor, R. E.; Kushon, S. A.; Wang, M.; Armitage, B. A. *J. Am. Chem. Soc.* **1999**, *121*, 2987. (b) Nunnally, B. K.; He, H.; Li, L. C.; Tucker, S. A.; McGown, L. B. *Anal. Chem.* **1997**, *69*, 2392. (c) Rettig, W.; Rurack, K.; Szczipan M. In *New trends in Fluorescence Spectroscopy. Applications to Chemical and Life Sciences*; Valeur, B., Brochon, J. C., Eds.; Springer-Verlag: Berlin, 2000.
- (12) (a) Jelly, E. E. *Nature* **1936**, *138*, 1009. (b) Scheibe, G. *Angew. Chem.* **1937**, *50*, 51; **1937**, *50*, 212. (c) Renge, I.; Wild, U. P. *J. Phys. Chem. A* **1997**, *101*, 7977.
- (13) Mandal, A. K.; Pal, M. K. *Chem. Phys.* **2000**, *253*, 115.
- (14) Meyer, Y. H.; Pittman, M.; Plaza, P. *J. Photochem. Photobiol. A* **1998**, *114*, 1.
- (15) Roth, N. J. L.; Craig, A. C. *J. Phys. Chem.* **1974**, *78*, 1154.
- (16) Sahyun, M. R.; Blair, J. T. *J. Photochem. Photobiol. A* **1997**, *104*, 179.
- (17) Fujimoto, Y.; Katayama, N.; Ozaki, Y.; Yasui, S.; Iriyama, K. *J. Mol. Struct.* **1992**, *274*, 183.
- (18) (a) Hofer, L. J. E.; Grabenstetter, R. J.; Wiig, E. O. *J. Am. Chem. Soc.* **1950**, *72*, 203. (b) Benson, R. C.; Kues, H. A. *J. Chem. Eng. Data* **1977**, *22*, 379.
- (19) Tredwell, C. J.; Keary, C. M. *Chem. Phys.* **1979**, *43*, 307.
- (20) Rentsch, S. K.; Danielius, R.; Gadonas, R. *Chem. Phys. Lett.* **1981**, *84*, 450.
- (21) (a) Levitus, M.; Martin Negri, R.; Aramendia, P. F. *J. Phys. Chem.* **1995**, *99*, 14231. (b) Martini, I.; Hartland, G. V. *J. Phys. Chem.* **1996**, *100*, 19764. (c) Chibisov, A. K.; Zakharova, G. *J. Chem. Soc., Faraday Trans.* **1996**, *92*, 4917. (d) Murphy, S.; Sauerwein, B.; Drickamer, H. G.; Schuster, G. B. *J. Phys. Chem.* **1994**, *98*, 13476. (e) Aramendia, P. F.; Martin Negri, R.; San Roman, E. *J. Phys. Chem.* **1994**, *98*, 3165.
- (22) Vogt, G.; Krampert, G.; Niklaus, P.; Gerber, G. personal communication.
- (23) (a) Kawasaki, M.; Inokuma, H. *J. Phys. Chem. B* **1999**, *103*, 1233. (b) Owen, D. J.; VenDerveer, D.; Schuster, G. B. *J. Am. Chem. Soc.* **1998**, *120*, 1705. (c) Laguitton-Pasquier, H.; Van der Auweraer, M.; De Schryver, F. C. *Langmuir* **1998**, *14*, 5172. (d) Botelho do Rego, A. M.; Penedo Pereira, L.; Reis, M. J.; Oliveira, A. S.; Vieira Ferreira, L. F. *Langmuir* **1997**, *13*, 6787.
- (24) (a) Mandal, A. M.; Pal, M. K. *Spectrochim. Acta A* **1999**, *55*, 1347. (b) Ghosh, J. K.; Mandal, A. K.; Pal, M. K. *Spectrochim. Acta A* **1999**, *55*, 1877.
- (25) Aramendia, P. F.; Martin Negri, R.; San Roman, E. *J. Phys. Chem.* **1994**, *98*, 3165.
- (26) Rulliere, C. *Chem. Phys. Lett.* **1976**, *43*, 303.
- (27) (a) Kasatani, K.; Sato, H. *Bull. Chem. Soc. Jpn.* **1996**, *69*, 3455. (b) Eske, A. T.; Razi N. K. *Chem. Phys. Lett.* **1979**, *63*, 128. (c) De Rossi, U.; Daehne, S.; Reisfeld, R. *Chem. Phys. Lett.* **1996**, *251*, 259.
- (28) Momicchioli, F.; Baraldi, I.; Berthier, G. *Chem. Phys.* **1988**, *123*, 103.
- (29) Sanchez-Galvez A.; Hunt, P.; Robb, M. A.; Olivucci, M.; Vreven, T.; Schlegel, H. B. *J. Am. Chem. Soc.* **2000**, *122*, 2911.
- (30) Cossi, M.; Rega, N.; Scalmani, M.; Barone, V. *J. Chem. Phys.* **2001**, *114*, 5691.
- (31) (a) Adamo, C.; Barone, V. *J. Chem. Phys.* **1999**, *110*, 6158. (b) Enzerhof, M.; Scuseria, G. E. *J. Chem. Phys.* **1999**, *110*, 5029.
- (32) Adamo, C.; Scuseria, G. E.; Barone, V. *J. Chem. Phys.* **2000**, *111*, 2889.
- (33) Improta, R.; Santoro, F.; Dietl, C.; Papastathoupolos, E.; Gerber, G. *Chem. Phys. Lett.* **2004**, *387*, 509.
- (34) Bearpark, M. J.; Robb M. A.; Schlegel, H. B. *Chem. Phys. Lett.* **1994**, *223*, 269.
- (35) Fantacci, S.; Migani A.; Olivucci M. *J. Phys. Chem. A* **2004**, *108*, 1208.
- (36) Barone, V.; Cossi, M.; Tomasi, J. *J. Chem. Phys.* **1997**, *107*, 3210.
- (37) Cossi, M.; Barone, V. *J. Chem. Phys.* **2001**, *115*, 4708.

- (38) Wiberg, K. B. *Tetrahedron* **1968**, *24*, 1083.
- (39) (a) Foster, J. P.; Weinhold, F. *J. Am. Chem. Soc.* **1980**, *102*, 7211. (b) Reed, A.; Weinhold, F. *J. Chem. Phys.* **1983**, *78*, 4066. (c) Glendening, E. D.; Weinhold, F. *J. Comput. Chem.* **1998**, *19*, 593.
- (40) Gaussian 03, Revision B.01, Frisch, M. J.; Trucks, G. W.; Schlegel, H. B.; Scuseria, G. E.; Robb, M. A.; Cheeseman, J. R.; Montgomery, J. A., Jr.; Vreven, T.; Kudin, K. N.; Burant, J. C.; Millam, J. M.; Iyengar, S. S.; Tomasi, J.; Barone, V.; Mennucci, B.; Cossi, M.; Scalmani, G.; Rega, N.; Petersson, G. A.; Nakatsuji, H.; Hada, M.; Ehara, M.; Toyota, K.; Fukuda, R.; Hasegawa, J.; Ishida, M.; Nakajima, T.; Honda, Y.; Kitao, O.; Nakai, H.; Klene, M.; Li, X.; Knox, J. E.; Hratchian, H. P.; Cross, J. B.; Adamo, C.; Jaramillo, J.; Gomperts, R.; Stratmann, R. E.; Yazyev, O.; Austin, A. J.; Cammi, R.; Pomelli, C.; Ochterski, J. W.; Ayala, P. Y.; Morokuma, K.; Voth, G. A.; Salvador, P.; Dannenberg, J. J.; Zakrzewski, V. G.; Dapprich, S.; Daniels, A. D.; Strain, M. C.; Farkas, O.; Malick, D. K.; Rabuck, A. D.; Raghavachari, K.; Foresman, J. B.; Ortiz, J. V.; Cui, Q.; Baboul, A. G.; Clifford, S.; Cioslowski, J.; Stefanov, B. B.; Liu, G.; Liashenko, A.; Piskorz, P.; Komaromi, I.; Martin, R. L.; Fox, D. J.; Keith, T.; Al-Laham, M. A.; Peng, C. Y.; Nanayakkara, A.; Challacombe, M.; Gill, P. M. W.; Johnson, B.; Chen, W.; Wong, M. W.; Gonzalez, C.; Pople, J. A. Gaussian, Inc.: Pittsburgh, PA, 2003.
- (41) Wanko, M.; Garavelli, M.; Bernardi, F.; Niehaus, T. A.; Frauenheim, T.; Elstner, M. *J. Chem. Phys.* **2004**, *120*, 1674.
- (42) Dreuw, A.; Weisman, J. L.; Head-Gordon, M. *J. Chem. Phys.* **2003**, *119*, 2943.
- (43) Ben-Nun, M.; Quenneville, J.; Martínez, T. J. *J. Phys. Chem. A* **2000**, *104*, 5161.
- (44) Besler, B. H.; Merz, K. M., Jr.; Kollman, P. A. *J. Comput. Chem.* **1990**, *11*, 431.
- (45) Zhang, T.; Chen, C.; Gong, Q.; Yan, W.; Wang, S.; Yang, H.; Jian, H.; Xu, G. *Chem. Phys. Lett.* **1998**, *105*, 236.
- (46) Åberg, U.; Åkesson, E.; Fedchenia, I.; Sundström, V. *Chem. Phys.* **1994**, *183*, 269.
- (47) Yartsev, A.; Alvarez, J.-L.; Åberg, U.; Sundström, V. *Chem. Phys. Lett.* **1995**, *243*, 281.
- (48) Xu, Q.-H.; Fleming, G. R. *J. Phys. Chem. A* **2001**, *105*, 10187.
- (49) Though the authors¹⁷ speak of a Resonance Raman experiment, we notice that at the 480 nm exciting wavelength they used, the absorption spectrum is vanishingly small. Therefore it is unlikely that any intermediate state is significantly populated, and at least the existence of a nonresonant contribution should be considered in assignment of the bands.
- (50) Rodríguez, J.; Sherlis, D.; Aramendía, P. F.; Negri, R. M. *J. Phys. Chem. A* **1997**, *101*, 6998.
- (51) Concerning the stCY vertical excitation, the agreement with experiment is deeply improved if the computation is performed at CASPT2 level of theory. See Schreiber, M.; Buss, V.; Fölscher, M. *Phys. Chem. Chem. Phys.* **2001**, *3*, 3906.

CT049899R